HHS Public Access

Author manuscript

Neurobiol Dis. Author manuscript; available in PMC 2022 March 01.

Published in final edited form as:

Neurobiol Dis. 2021 March ; 150: 105246. doi:10.1016/j.nbd.2020.105246.

Increased glutamate transmission onto dorsal striatum spiny projection neurons in *Pink1* knockout rats

Rose B. Creed[1,2], **Rosalinda C. Roberts**[5], **Charlene B. Farmer**[5], **Lori L. McMahon**[1,2,4,*], **Matthew S. Goldberg**[1,2,3,*]

[1]Center for Neurodegeneration and Experimental Therapeutics, the University of Alabama at Birmingham, Birmingham, Alabama 35294

[2]Department of Neurology, the University of Alabama at Birmingham, Birmingham, Alabama 35294

[3]Department of Neurobiology, the University of Alabama at Birmingham, Birmingham, Alabama 35294

[4]Department of Cell, Developmental, and Integrative Biology, the University of Alabama at Birmingham, Birmingham, Alabama 35294

[5]Department of Psychiatry and Behavioral Neurology, the University of Alabama at Birmingham, Birmingham, Alabama 35294

Abstract

Loss-of-function *PTEN Induced Kinase 1 (PINK1)* mutations cause early-onset familial Parkinson's disease (PD) with similar clinical and neuropathological characteristics as idiopathic PD. While *Pink1* knockout (KO) rats have mitochondrial dysfunction, locomotor deficits, and α-synuclein aggregates in several brain regions such as cerebral cortex, dorsal striatum, and substantia nigra, the functional ramifications on synaptic circuits are unknown. Using whole cell patch clamp recordings, we found a significant increase in the frequency of spontaneous excitatory postsynaptic currents (sEPSCs) onto striatal spiny projection neurons (SPNs) in *Pink1* KO rats at ages 4 and 6 months compared to wild-type (WT) littermates, suggesting increased excitability of presynaptic neurons. While sEPSC amplitudes were also increased at 2 and 4 months, no changes were observed in AMPAR/NMDAR ratio or receptor expression. Further analysis revealed increased glutamate release probability and decreased recovery of the synaptic vesicle pool following a train of stimulation in *Pink1* KO rats. Ultrastructural analysis revealed increased excitatory and inhibitory synapse number and increased levels of presynaptic α- synuclein, while the number and structure of striatal mitochondria appeared normal. Lastly, we found that *Pink1* KO rats have altered striatal dopamine tone, which together with the abnormal α- synuclein distribution and dysfunctional mitochondria, could contribute to the increase in excitatory

*Co-corresponding Authors mattgoldberg@uabmc.edu, mcmahon@uab.edu.

The authors declare no conflict of interest

transmission. Together, these studies show that PINK1 is necessary for normal glutamatergic transmission onto striatal SPNs and reveal possible mechanisms underlying striatal circuit dysfunction in PD.

Keywords

Dorsal striatum; PINK1; Parkinson's disease; excitatory transmission

Introduction

Parkinson's disease (PD) is the most common neurodegenerative motor disorder. Clinically, PD patients present with motor symptoms including bradykinesia, resting tremor, and postural instability. Histologically, PD is characterized by loss of dopaminergic neurons of the substantia nigra pars compacta (SNpc) and the presence of α- synuclein enriched proteinaceous inclusions termed Lewy bodies and Lewy neurites (Spillantini et al., 1997; Spillantini et al., 1998). While most PD cases are idiopathic, 5–10% of cases are familial with recessive mutations in the *PTEN Induced Kinase 1 (PINK1)* gene accounting for a subset of those cases (Valente et al., 2004b; Valente et al., 2004a).

The mechanism by which loss-of-function of the PINK1 protein causes PD is not well understood. PINK1 is a mitochondrial targeted kinase involved in a myriad of functions such as removal of damaged mitochondria (Kane et al., 2014; Lazarou et al., 2015; Truban et al., 2017), maintenance of mitochondrial calcium homeostasis (Heeman et al., 2011), mitochondrial bioenergetics (Rango et al., 2020), and recently has been implicated in misfolded protein clearance (Du et al., 2017), and neuronal branching (Dagda et al., 2014). While *Pink1* KO drosophila and mouse models have provided valuable insights regarding the function of PINK1, they fail to reproduce relevant PD phenotypes. Compared to other animal models, *Pink1* KO rats reproduce more PD-relevant locomotor behavior deficits, α-synuclein neuropathology, and nigrostriatal degeneration (Dave et al., 2014; Grant et al., 2015; Creed and Goldberg, 2019; De Haas et al., 2019), providing a framework with which to link mechanistic findings with motor function. Because onset of PD motor symptoms occurs only after significant loss of SNpc dopamine neurons (Cheng et al., 2010), the appearance of locomotor impairments in *Pink1* KO rats prior to reported nigral cell loss merits investigation. Evidence suggest that preferential activation of striatal spiny projection neuron (SPN) subtypes is enough to result in hypokinetic or PD-like motor impairments in mice (Kravitz et al., 2010). This raises the question of whether excitatory neurotransmission onto striatal SPNs is altered in *Pink1* KO rats. Interestingly, unique to *Pink1* KO rats and concurrent with impaired locomotion is the early presence of endogenous α- synuclein pathology and mitochondrial abnormalities (Stauch et al., 2016a; Stauch et al., 2016b; Villeneuve et al., 2016), two factors known to affect neurotransmission.

Investigations of striatal circuitry in *Pink1* KO mice have revealed deficits in long-term synaptic plasticity resulting from impaired dopamine release (Kitada et al., 2007; Madeo et al., 2014; Schirinzi et al., 2016). While these studies have inferred altered glutamate release, it is surprising that there is a lack of detectable change in the frequency or amplitude of

spontaneous or miniature excitatory postsynaptic currents (sEPSCs) in *Pink1* KO mice (Kitada et al., 2007; Martella et al., 2009), as these are measures of basal synaptic glutamate transmission onto SPNs. To our knowledge, only a single report exists showing increased spontaneous excitatory transmission in *Pink1* KO mice, occurring at hippocampal synapses rather than in striatum (Feligioni et al., 2016); no change in long-term synaptic plasticity was detected at hippocampal synapses in contrast to striatum in those mice (Kitada et al., 2007; Feligioni et al., 2016). Therefore, the effect of loss of PINK1 function on synaptic glutamate release onto striatal SPNs requires further investigation. SPNs are mostly quiescent under basal conditions, necessitating excitatory synaptic inputs to increase activity and fire action potentials (Wilson and Kawaguchi, 1996). Interestingly, *in vivo* recordings from PD patients show robust increases in SPN firing frequency (Singh et al., 2016), presumably due to increased excitatory drive. Additionally, increased synaptic glutamate transmission onto striatal SPNs has been observed in dopamine depleted, 6-OHDA models of PD (Calabresi et al., 1993; Tang et al., 2001; Gubellini et al., 2002). These findings, however, do not explain the early occurrence of locomotor abnormalities in *Pink1* KO rats in the absence of nigral cell loss or a decrease in striatal dopamine (Dave et al., 2014; Creed et al., 2019).

To more directly investigate whether glutamatergic release onto SPNs of *Pink1* KO rats is altered compared to littermate controls, we performed whole-cell patch clamp electrophysiological, ultrastructural, and biochemical analyses at ages spanning before and after motor symptoms appear. We found that *Pink1* KO rats have increased excitatory transmission onto striatal spiny neurons. We also detected enhanced presynaptic release in *Pink1* KO rat striatum at 4 months of age, when the reported motor abnormalities are just beginning to occur. Ultrastructural analysis using electron microscopy revealed overall increases in excitatory and inhibitory synapse number in dorsal striatum even though no change in maximal connectivity was detected in input/output electrophysiology recording. Further anatomical analysis revealed no changes in mitochondrial number or structure. Finally, we explored various mechanisms that may underlie the observed increase in excitatory transmission in *Pink1* KO rats. Overall, our data reveal synaptic dysfunctions in *Pink1* KO rats and provide insights into possible mechanisms by which loss of PINK1 function could contribute to circuit abnormalities in PD.

Materials and Methods

Animals

All experiments were performed in accordance with the National Institutes of Health Guide for the Care and Use of Laboratory Animals and with the approval of the University of Alabama at Birmingham Institutional Animal Care and Use Committee. *Pink1* KO rats, on a Long-Evans genetic background, were obtained with a breeding license from Horizon Discovery and bred in our colony to obtain homozygous KO and WT littermate controls. Male rats were used for all experiments. Animals were provided food and water *ad libitum* and maintained on a 12-hour light/dark cycle with lights on at 6 AM.

Striatal slice preparations and electrophysiology recordings

Rats were anaesthetized with isoflurane, and rapidly decapitated between 7 and 8 AM. Acute coronal slices were obtained from 2, 4, and 6 month old WT and *Pink1* KO littermate controls. Slices were cut using a vibratome (Leica VT 1000P) at a thickness of 400 μm, in ice cold, high sucrose, artificial cerebral spinal fluid (aCSF) (in mM: 85.0 NaCl, 2.5 KCl, 4.0 $MgSO_4$ * 7 H_20, 0.5 CaCl* 2 H_20, 1.25 NaH_2PO_4, 25 $NaHCO_3$, 25 Glucose, 75 Sucrose). Slices were allowed to recover in a submersion chamber for at least one hour in regular aCSF (in mM: 119 NaCl, 2.5 KCl, 1.3 $MgSO_4$ * 7 H_20, 2.5 CaCl* 2 H_20, 1.0 NaH_2PO_4, 26 $NaHCO_3$, 11 Glucose, 2 Kynurenic Acid) at room temperature prior to recordings. Slices were kept oxygenated throughout the experiments with bubbling carbogen (5% CO_2/ 95% O_2).

Whole-cell patch clamp recordings were obtained from spiny projection neurons (SPNs) in the dorsal striatum. Data were collected with an Axopatch 200B amplifier, Digidata 1440A (Molecular devices), and using Clampex 10.3 (pClamp; Molecular Devices, San Jose, CA). All recordings were acquired in voltage clamp and were low-pass filtered at 5 kHz and digitized at 10 kHz.

All recordings were obtained with a cesium gluconate internal solution (in mM: 100 50% gluconic acid, 0.6 EGTA, 5.0 $MgCl_2$, 2.0 ATP, 0.3 GTP, 40 HEPES, pH to 7.2 with CsOH, 5 QX-314). Because all experiments were measuring glutamatergic transmission, 100μM picrotoxin (Sigma) was included in the perfusion aCSF to block $GABA_A$ receptor mediated inhibitory transmission. Spontaneous and miniature excitatory post synaptic currents (sEPSCs and mEPSCs, respectively) were recorded at a holding voltage of −80 mV. For mEPSCs, action potentials were blocked with 1μM tetrodotoxin (TTX; Tocris).

Evoked EPSCs (eEPSCs) were generated with a bipolar nichrome electrode placed in the corpus callosum, to access the corticostriatal fibers, parallel to the patch pipette in the dorsal striatum. To determine AMPAR/NMDAR ratios, neurons were recorded at a holding voltage −20 mV to relieve the voltage-dependent magnesium block of NMDARs. After obtaining a stable baseline, 5 μM CPP (Tocris) was washed on to block NMDAR currents and isolate AMPAR currents for 15 min. The remaining AMPAR current was blocked using 10μM DNQX (Sigma), and the AMPAR/NMDAR ratio was calculated by subtraction from total current. To obtain basal synaptic strength, input-output relationships were measured by increasing the stimulus intensity by 0.5 μA from a zero current baseline until maximum current was elicited.

To assess presynaptic release probability, pairs of pulses were delivered at 25, 50, 100, or 150 millisecond (ms) inter-stimulus intervals. Paired pulse ratios were calculated by dividing the amplitude of the second EPSC by that of the first EPSC at each inter-stimulus interval. Synaptic vesicle recycling was measured by eliciting a 50Hz stimulus train (20 pulses, 400ms) followed by individual pulses at 10, 25, 50, 100, 500, 4000, 8000 ms following the train. Percent recovery was calculated by dividing the amplitude of each evoked current by the amplitude of the first evoked current in the train, multiplied by 100.

Biochemistry

Striatal dissection and synaptosomal preparation—Brains were harvested and the striatum was dissected on ice, then frozen. Synaptosomes were isolated according to a modified protocol (Hallett et al., 2008). Briefly, striatal tissue from WT and *Pink1* KO littermates was homogenized in TEVP buffer (10mM Trish, PH 7.4, 5mM NaF, 1mM EDTA, 1mM EGTA, 1mM Na3VO4) containing 320mM sucrose using a dounce homogenizer and centrifuged for 10 min at 800 x g at 4°C. Supernatant was centrifuged for 15 min at 9,200 x g at 4°C, following which the supernatant was decanted into a clean eppendorf tube. The pellet was resuspended in TEVP buffer containing 35.6 mM sucrose and was gently vortexed to dislodge the pellet, then incubated on ice for 30 min. Vortexed samples were centrifuged for 20 min at 25,000 x g. The resulting pellet, comprised of synaptosomal membranes, was resuspended in TEVP buffer. All buffers contained protease and phosphatase inhibitor cocktails (Sigma).

Western Blotting—For gel electrophoresis, equal amounts of protein, measured by BCA assay, were mixed with Laemelli buffer and separated on a 4–20% mini-protean gel (Bio-rad). Proteins were then transferred onto a 0.2 μM PVDF membrane. Following transfer, membrane was blocked using 1:1 odyssey blocking buffer (LI-COR) and TBS with 0.05% tween-20 (TBS-T) for 1 hour at RT. Membranes were incubated with primary antibody overnight at 4°C: GluR2, 1:1,000, Antibodies Inc.; NR2B, 1:1000, Neuromab; GAPDH, 1:5,000, Millipore. Membranes were then incubated with LI-COR odyssey secondary antibodies in blocking buffer for 2 hours RT and imaged using LI-COR Odyssey CLx scanner.

Electron microscopy

Isoflurane anesthetized 4-month old WT (N=4) and *Pink1* KO rats (N=4) were transcardially perfused with 1X PBS, then brains were removed and hemisected. Right hemispheres were designated for electron microscopy and were immersed in a cold solution of 4% paraformaldehyde and 1% glutaraldehyde in 0.1M Phosphate Buffer (PB), pH 7.4. Emersion fixation was selected as we have done previously (Perez-Costas et al., 2010; Roberts et al., 2014; Warmus et al., 2014) in order to preserve a hemisphere for non-anatomical studies. After two days of fixation, the striatum from all rats was cut at 40μm thickness using a vibratome (Microm HM 650V) and stored in 0.1 M PB at 4°C.

For DAB immunohistochemistry (IHC), sections were washed 6 ×5 min in phosphate buffered saline (1X PBS) and blocked in 1% normal goat serum (NGS) in 1X PBS for 1 hour RT. Sections were then incubated in anti-α- synuclein primary antibody (1:500, CST #4179) overnight at 4°C. Sections were washed in 1X PBS followed by incubation in biotinylated goat anti-rabbit secondary antibody (1:500, vector) for 2 hours RT. Following 3×5 minute washes in 1X PBS, sections were incubated in ABC solution (vector) for 2 hours, washed three times in PBS, then incubated in DAB solution for approximately 3 minutes. Following 3 washes in 1X PBS, sections were mounted onto slides, dried and coverslipped for light microscopy, while the remaining sections were prepared for EM. Controls consisted of omitting the primary antibody, but otherwise processing the tissue identically. All the samples were processed for immunohistochemistry on the same day.

Sections processed for IHC and non-immunolabeled sections were flat embedded as previously described in (McCollum et al., 2015). The tissue sections were processed for EM on the same day for all IHC sections and on a different day for all of the non-IHC sections. Briefly, following washes in 0.1 M PB, tissue was incubated for 1hr in 1% osmium tetroxide (OsO_4). Sections were then thoroughly rinsed with 0.1 M PB followed by subsequent 50 and 70% ethanol rinses. Sections were then incubated in 1% uranyl acetate solution for 1 hour in the dark followed by two 70% ethanol rinses then stored overnight in the dark. Sections were next dehydrated with 95 % ethanol (3 × 5min), followed by rinses with 100% ethanol (3 × 5 min) then 100% propylene oxide (2 × 10 min). Next, sections were set in 1:1 epon resin: propylene oxide for 1 hour, followed by 2: 1 epon resin: propylene oxide for 1 hour and finally, in 100% epon resin for 3 hours. Sections were then mounted on EM-pretreated slides and left to polymerize for 72 hours at 60°C. Upon polymerization, a $1mm^2$ block from dorsal striatum was taken from each mouse and thin-sectioned at 90nm on an ultramicrotome (Leica EM UC6). These sections were collected onto copper grids (EMS, FCF2010-CU) for EM imaging.

A Hitachi H-7650 transmission electron microscope was used to view EM tissue, and micrographs were taken with a Hamamatsu Orca-HR digital camera. All micrographs were taken at the same accelerating voltage of 80KV. For each rat, 20 electron micrographs of neuropil were taken at random at 15,000X magnification; each micrograph was $110\mu m^2$. Electron micrographs were then analyzed in Photoshop at 50 % magnification. Synapses were identified by the following criteria: 1) a presynaptic terminal with at least three synaptic vesicles at the cleft, 2) parallel pre and post synaptic membranes with light density within the cleft, and 3) a postsynaptic density. All synapses were counted and subcategorized as excitatory or inhibitory based on morphological features (Gray, 1969). Synapses with thin postsynaptic densities were designated as symmetric (Type II) and inhibitory, and those with thick postsynaptic densities were designated as asymmetric (Type I) and excitatory. The numbers of Type I and II synapses were counted and averaged across 20 micrographs per animal. The length of the active zone of type I synapses was measured using Image J.

For IHC sections, electron micrographs of immunolabeled axon terminals were taken at 30,000X magnification within the same zone from the surface of the 40 micron thick sections and in the region of optimal immunoreactivity; that is not on the edge, but in a region where immunoreactivity was present in the neuropil. Axon terminals containing α-synuclein labelling were counted in Photoshop. The density of immunolabeling in all labeled terminals was quantified using image J. For each electron micrograph, an area without tissue (such as the lumen of a capillary, or a location off the tissue) was measured and used as background. Then, the immunolabeled terminal was traced with the wand tool excluding mitochondria. The OD of the background in each micrograph was subtracted from each labeled terminal. The individuals acquiring the photomicrographs, performing the synapse counting, and density quantification were blind to the genotypes.

Data analysis and statistics

Data were analyzed and graphs were generated using Graph pad prism 8 and are represented as mean +/− SEM. Data were tested for normality and appropriate parametric tests were performed. Where data failed to show a normal distribution, appropriate non-parametric tests were performed.

Results

Spontaneous EPSCs onto SPNs is increased in *Pink1* KO rats

To determine whether *Pink1* KO rats have increased glutamate transmission, we used whole-cell patch clamp recordings in acute coronal slices to measure sEPSCs onto dorsal striatal spiny neurons (Figure 1A). In our coronal slices, glutamatergic innervation from the cortex remain intact (Hunnicutt et al., 2016). We detected a slight leftward shift in the inter-event interval (increase in frequency) of sEPSCs in slices from rats at age 2 months, with a significant increase in sEPSC amplitude (rightward shift in the cumulative distribution curve) from *Pink1* KO rats compared to controls (Figure 1B). At age 4 months, both sEPSC amplitude (rightward shift in the cumulative distribution curve) and frequency (leftward shift in the cumulative distribution curve) were robustly increased in *Pink1* KO rats (Figure 1C). When measured from rats at age 6 months, the decrease in inter-event interval (increase in frequency) of sEPSC was still present in *Pink1* KO rats albeit to a lesser extent than at age 4 months; however, no visible shift of the curves was observed between genotypes in sEPSC amplitude in slices from rats at age 6 months (Figure 1D).

To determine whether the significant increases in sEPSC frequency and amplitude observed at age 4 months were pre- or post-synaptically mediated, we measured miniature EPSCs (mEPSCs) in the presence of tetrodotoxin (TTX, 1μM) to block action potential mediated events. In the presence of TTX, the difference between WT and *Pink1* KO rats in inter-event interval was eliminated and only a very slight, yet still statistically significant, difference in amplitude remained (Figure 1E). These results indicate that the increases observed in sEPSC frequency is action potential dependent and consistent with a presynaptic mechanism.

No change in AMPA/NMDA ratio or receptor expression *Pink1* KO rats

Although the findings above suggest a presynaptic mechanism underlies the increase in sEPSC frequency in *Pink1* KO rats at age 4 months, we wanted to determine whether a postsynaptic mechanism may also have a role. To this end, we used whole-cell voltage clamp recordings of SPNs and electrically evoked EPSCs by stimulating in the corpus callosum in the presence of pharmacological inhibition of $GABA_A$ receptors (Figure 2A). AMPAR and NMDAR currents were pharmacologically isolated and analysis showed no detectable changes in the AMPAR/NMDAR current ratio, suggesting that there was not a selective increase in AMPAR or NMDAR transmission that was contributing to the increase in sEPSC amplitude (Figure 2B–C). Next, we used Western blot analysis to measure the protein levels of GluA2 AMPAR subunits and GluN2B NMDAR subunits and found no differences between WT and *Pink1* KO rat striatum (Figure 2D–E). These data indicate that the observed increases in sEPSC amplitude in *Pink1* KO rats are not due to increased postsynaptic current through AMPAR and NMDARs.

Pre-synaptic release is increased in *Pink1* KO rats

To further investigate the extent to which the increases in glutamatergic transmission were pre-synaptically mediated, we measured paired-pulse ratios (PPR), an indirect measure of presynaptic release probability (Dobrunz and Stevens, 1997) at 25, 50, 100, and 150ms inter-stimulus intervals (ISI), stimulating within the corpus callosum to primarily activate corticostriatal synapses. There was no difference in PPR between in WT and *Pink1* KO rats at ages 2 (Figure 3A–B) or 6 months (Figure 3E–F). However, PPR was significantly decreased at the 100ms ISI in *Pink1* KO rats at age 4 months (Figure 3C–D), consistent with an increase in release probability.

As a second approach, we measured the rate of block of synaptically activated NMDARs in WT and *Pink1* KO rats at age 4 months using the open channel blocker MK801. Following application of MK-801, NMDAR current amplitudes were normalized to baseline and the curves were fitted with a first order exponential (Speed and Dobrunz, 2009). This revealed a faster rate of block (steeper slope) of synaptically activated NMDARs in recordings of SPNs from *Pink1* KO rats compared to WT rats (Figure 3G–H). Collectively, these data indicate increased presynaptic glutamate release at corticostriatal synapses onto SPNs in *Pink1* KO rats.

Given the importance of PINK1 to mitochondrial quality control, as well as the substantial energy requirement of synaptic vesicle recycling, we hypothesized that impairments in vesicle cycling at corticostriatal synapses may underlie the observed increase in glutamate release. To test this, we electrically stimulated the corticostriatal fibers with a 50Hz stimulus train followed by a single pulse at specific time intervals (range 10ms- 8s) following each train to assess recovery of transmission onto the SPNs (Figure 4A). To determine the maximum current generated during the stimulus train, we analyzed the total area under the curve (AUC) and observed no significant difference between recordings in WT and *Pink1* KO slices from rats at ages 2 and 6 months (Figure 4B, D). Interestingly, at age 4 months, the stimulus train generated a greater maximum current in recordings of SPNs from *Pink1* KO rats compared to WT (Figure 4C). As expected from the apparent greater release during the train, 4 month old *Pink1* KO rats had a deficit in the recovery percentage (smaller current amplitude of the single eEPSC) at each interval except 4 and 8s, compared to WT littermates. In contrast, 2 and 6 month old *Pink1* KO rats showed no change in the EPSC amplitude recovery at any interval (Figure 4B–D, right), consistent with similar release during the train as evidenced by no difference in maximum current generated.

Increase in number of excitatory and inhibitory synapses in the striatum

The extensive synaptic abnormalities in *Pink1* KO rats at age 4 months prompted us to explore possible driving mechanisms. To determine whether structural alterations to striatal axon terminals could contribute to the observed increases in sEPSC frequency and amplitude in the *Pink1* KO rats, we used electron microscopy (EM) to measure the abundance and structure of synapses in the dorsal striatum of *Pink1* KO rats and WT littermate controls (Figure 5A–B). We observed an increase in the number of total active zones (excitatory and inhibitory; Figure 5C) which was driven by individual increases in the numbers of excitatory and inhibitory active zones (Figure 5D, F) in *Pink1* KO rat striatum. No changes were

observed in the excitatory active zone length (Figure 5E). When the data were treated as a single value for each animal (mean of all the measurements from that animal), we found a significant increase in the number of inhibitory synapses per area in *Pink1* KO rats, but no other significant differences (Figure 5G–J).

To determine whether the increase in excitatory active zone number corresponded with a functional increase in basal synaptic strength in *Pink1* KO rats, we measured input-output relationships using whole-cell voltage clamp of SPNs with increasing stimulus intensity in acute slices from *Pink1* KO rats and WT littermate controls (Figure 5K) and detected no change in the strength of maximal transmission (Figure 5L), suggesting that the observed increase in excitatory active zone number does not drive an increase in basal synaptic strength.

Because PINK1 is known to target dysfunctional mitochondria for degradation by mitophagy, we investigated whether *Pink1* KO rats had abnormal morphology or number of striatal mitochondria. Using EM, we observed no apparent ultrastructural abnormalities of presynaptic mitochondria in *Pink1* KO rats compared to WT rats (Figure 6A–C). Additionally, no differences were observed, either by distribution or by averages, in mitochondrial number (Figure 6D–F).

The previously reported increases in synaptic vesicle-associated α- synuclein in the cortex of *Pink1* KO rats (Creed and Goldberg, 2019) prompted us to ask whether the distribution of synaptic α- synuclein was altered in *Pink1* KO striatum, which could underlie the observed increases in glutamatergic release. To visualize the α- synuclein protein distribution in synapsing axons within the striatum, we performed DAB immunohistochemistry using an antibody specific for α- synuclein, and then processed the sections for EM (Figure 7A). Negative control sections in which the primary antibody was omitted showed no α- synuclein positive immunoreactivity (Figure 7B). We found no significant differences in the average number of dorsal striatal axon terminals positive for α- synuclein immunoreactivity in *Pink1* KO compared to WT rats (Figure 7C). Optical density (OD) analysis revealed a decrease in both the distribution (Figure 7D) and the average (Figure 7E) α- synuclein immunoreactivity of axon terminals in *Pink1* KO rats compared to WT littermate controls.

Decreased effect of dopamine receptor antagonism on evoked AMPAR currents in *Pink1* KO rats

Dopamine suppresses glutamatergic transmission in the striatum by binding to D2-type receptors located on presynaptic terminals of glutamatergic afferents (Tritsch and Sabatini, 2012; Surmeier et al., 2017) (Figure 8, A). Under normal conditions, pharmacological inhibition of presynaptic dopamine receptors results in an increase in the amplitude of evoked AMPAR current due to relief of dopamine tone that decreases glutamate release (Bamford, 2004). However, if dopamine tone is lost or decreased due to degeneration or dysfunction of dopaminergic axons, blocking dopamine receptors would be less effective at increasing evoked AMPAR current amplitude recorded from SPNs. Therefore, we determined whether the amplitude of evoked AMPAR currents recorded from WT and *Pink1* KO rats are differently modulated by dopamine receptor antagonism as an indirect measure of extracellular dopamine acting on dopamine receptors. We applied a dopamine receptor

inhibitor cocktail containing the D1 receptor antagonist SCH23390 (3μM; Tocris) and the D2 receptor antagonist sulpiride (10μM; Sigma) on acute striatal slices (Figure 8B). Stimulating within the corpus callosum, we measured eEPSC amplitudes before and after application of dopamine receptor blocker cocktail (Figure 8C). In slices from WT rats, we observed the expected increase in the amplitude of eEPSCs following application of the inhibitor cocktail (Figure 8D, left). By contrast, in recordings from *Pink1* KO, rats no significant increase in eEPSC amplitude was detected following inhibitor cocktail application (Figure 8D, right). Additionally, in a second experiment, we stimulated within dorsal striatum (Figure 8E) and again observed an increase in WT eEPSC amplitude following dopamine inhibitor cocktail application (Figure 8F, left) with no change in *Pink1* KO slices (Figure 8F, right). The lack of a net increase in eEPSC amplitude in *Pink1* KO rats, irrespective of stimulation site, could be indicative of a decrease in striatal dopamine tone or loss of dopamine mediated neuromodulation.

Discussion

In the present study, we sought to determine the extent to which PD-linked PINK1-deficiency affects excitatory synaptic transmission onto striatal SPNs, the major site of dysfunction in PD. We utilized the *Pink1* KO rat model, in which previous neurochemical analyses revealed increased striatal glutamate and glutamine levels (Ren et al., 2019). Our results show increased glutamate release onto SPNs of *Pink1* KO rats, indicating that the previously described increases in glutamate could be a consequence of this heightened synaptic transmission. Analysis of mEPSCs to determine whether a pre-or post-synaptic mechanism underlies the increase in sEPSC frequency and amplitude revealed the increase in frequency to be action potential dependent as no difference in mEPSC frequency was observed when compared to WT littermate controls. These results are consistent with findings from 6-OHDA neurotoxin and mutant *Leucine Rich Repeat Kinase 2 Knock*-in models of PD (Calabresi et al., 1993; Tang et al., 2001; Gubellini et al., 2002; Matikainen-Ankney et al., 2016; Volta et al., 2017). Additionally, Our results may provide mechanistic insights into reported increases in activity patterns of SPNs from both parkinsonian non-human primates and PD patients (Singh et al., 2016). The absence of differences in the protein levels of AMPAR and NMDAR subunits in WT versus *Pink1* KO rats at age 4 months suggests that the observed increases in amplitudes, specifically at 4 months, could be driven by increased activity of the presynaptic glutamatergic neurons. However, these observations do not rule out postsynaptic changes in the function or expression of AMPAR and NMDAR, and do not exclude possible post synaptic impairments in *Pink1* KO rats.

Our investigation of whether the heightened glutamate transmission is pre-synaptically mediated revealed increased release probability, increased release during a high frequency train, and slower recovery of evoked transmission following the train. The increase in release probability was only detected at the 100ms ISI, and while this observation is atypical, similar observations have been made in other PD models (Guatteo et al., 2017). Interestingly, these changes were only detectable at 4 months of age, which correlates with the onset of reported locomotor abnormalities in *Pink1* KO rats (Dave et al., 2014). However, behavioral abnormalities in *Pink1* KO rats persist at ages 6 months and beyond (Dave et al., 2014; De Haas et al., 2019), which is seemingly at odds with our data showing

normal presynaptic release at age 6 months. One likely explanation is homeostatic plasticity resulting in normalization of any changes in presynaptic release by age 6 months. Interestingly, *Pink1* KO rats were reported to have an increase in D2 dopamine receptor density at 6 month of age (Sun et al., 2013). This increase in density at 6 months could be a compensatory response from decreased D2 receptor efficacy consistent with our observed apparent functional impairment of dopamine mediated neuromodulation at 4 months. This same decrease in D2 receptor efficacy, possibly due to loss of dopamine tone, may also partly underly the increases in presynaptic release observed at 4 months. Additionally, our data indirectly showing impaired dopamine mediated neuromodulation in *Pink1* KO rats is consistent with the deficits in long-term synaptic plasticity in *Pink1* KO mice (Kitada et al., 2007; Madeo et al., 2014), and likely predicts deficits in long term plasticity in *Pink1* KO rats. Moreover, the increased sEPSC frequency in *Pink1* KO rats at age 6 months indicates a persistence of dysfunction in the striatal circuit; which aside from compensatory changes, could also be driven by increased release from other striatal input nuclei such as the thalamus.

While our ultrastructural analysis showed increases in the number of excitatory synapses within the striatum of *Pink1* KO rats, there was no detectable electrophysiological consequences on basal synaptic strength. These observations are consistent with the absence of change in mEPSC frequency which should be increased if there was an increase in the number of functional synapses, and further support our conclusion that the increased glutamate release at 4 months is driven by increased activity of the presynaptic neurons. Of interest, two recent studies suggest possible explanations for the increased number of synapses in *Pink1* KO rats. The first, conducted in *Pink1* KO mice, provides evidence that lack of PINK1 results in impaired caspase mediated synaptic pruning (Imbriani et al., 2019). The second implicates a role for astrocytes in the dopaminergic system whereby the astrocytes respond to synaptically released dopamine and ultimately depress excitatory transmission on SPNs (Corkrum et al., 2020). This phenomenon, in light of reported enrichment of PINK1 activity in astrocytes (Barodia et al., 2019), could underlie our observed increases in both excitatory synapse number, as astrocytes actively contribute to activity dependent synaptic pruning (Chung et al., 2015), and excitatory transmission in *Pink1* KO rats. While loss of PINK1 function in glial cell types has been linked to a pathological innate immune response (Sun et al., 2018), these recent findings, coupled with our current data showing impaired dopamine tone and increased glutamate transmission in the striatum, implicate a much greater involvement of PINK1 in maintaining the normal function of the striatal circuit.

Our observed increase in inhibitory active zone number suggests that further functional investigations of the inhibitory network in *Pink1* KO rats are warranted. Electrophysiological analyses of aged *Pink1* KO mice showed altered $GABA_A$ receptor transmission (Dehorter et al., 2012), similar to what is seen in the 6-OHDA mouse model of PD (Gittis et al., 2011). The pathological increase in beta oscillations observed in the striatum of PD patients are partly the result of enhanced $GABA_A$ receptor currents (McCarthy et al., 2011). In the present study, all recordings were acquired in the presence of $GABA_A$ receptor blockers and therefore the contributions of $GABA_A$ transmission onto

SPNs in *Pink1* KO rats remains unknown. *Pink1* KO rats could be a useful model to explore this in order to better understanding the network dysfunction in PD.

The spontaneous appearance of aggregates of endogenous α- synuclein is another PD-relevant feature of *Pink1* KO rats (Grant et al., 2015; Creed and Goldberg, 2019). Our EM results following DAB immunohistochemistry indicate further changes in the distribution of α- synuclein at presynaptic terminals in the striatum of *Pink1* KO rats. While no change was found in the overall number of labelled axon terminals, there was a decrease in the optical density of α- synuclein immunoreactivity in axon terminals in the striatum of *Pink1* KO rats compared to WT. We interpret the decrease in optical density (leftward shift of the cumulative distribution) of α- synuclein immunoreactivity in *Pink1* KO rats to potentially indicate a shift in the biophysical state of α- synuclein. The decreased optical density may correspond to more membrane bound or structured forms of α- synuclein in which the epitope is less accessible, as opposed to more unbound or unstructured α- synuclein in which the epitope is more accessible to the antibody in WT rats. This is consistent with our previously published biochemical analysis of WT and *Pink1* KO rat brains showing a significant shift of α- synuclein from the unbound cytosolic fraction to the synaptic vesicle-enriched fraction in *Pink1* KO rats, even though the total α- synuclein protein levels are unchanged (Creed and Goldberg, 2019). In line with our observations, studies show α-synuclein normally acts as an attenuator of neurotransmission by restricting mobilization of synaptic vesicles (Scott and Roy, 2012; Wang et al., 2014; Sun et al., 2019). Therefore, a change in the biochemical state of α- synuclein in axon terminals within the striatum of *Pink1* KO rats may reflect a greater percentage of untethered presynaptic vesicles, consistent with our observed increase in neurotransmission. Additionally, the leftward shift in α-synuclein density at the presynaptic terminals in the striatum of *Pink1* KO rats could be related to our observed increase in glutamate release. Increasing concentration of extracellular calcium, an important driver in presynaptic release, is shown to promote secretion of α- synuclein (Emmanouilidou et al., 2010). Therefore, as our data indicate increased release from presynaptic terminals in the striatum of *Pink1* KO rats, α- synuclein could be co-released, decreasing the apparent density within presynaptic terminals.

Together, our data indicate that loss of function of PINK1 leads to increased synaptic glutamate release onto striatal SPNs and that this increase is likely due to increased firing of glutamatergic presynaptic neurons. This increased release could be driven by a number of mechanisms such as α-synuclein dyshomeostasis or loss of dopamine tone in *Pink1* KO rats. Further analyses are needed to determine the extent to which these results are a consequence of compensatory mechanisms or directly due to loss of PINK1 function within neurons, or potentially within non-neuronal cells, such as astrocytes. Our findings highlight the potential utility of *Pink1* KO rats both for studying the normal function of PINK1 in synaptic physiology and for ultimately identifying the as yet unknown mechanisms by which human mutations in *PINK1* cause the clinical and neuropathological features of PD.

Acknowledgement:

This study was supported by grants from NIH/NIA/NINDS F99NS108458 to RBC, and by grants 11380 from the Michael J. Fox Foundation for Parkinson's Research and NIH/NINDS R01NS082565 to MSG.

References

Bamford NS, Zhang H, Schmitz Y, Wu N-P, Cepeda C, Levine MS, Schmauss C, Zakharenko SS, Zablow L, Sulzer D (2004) Heterosynaptic Dopamine Neurotransmission Selects Sets of Corticostriatal Terminals. Neuron 42:653–663. [PubMed: 15157425]

Barodia SK, McMeekin LJ, Creed RB, Quinones EK, Cowell RM, Goldberg MS (2019) PINK1 phosphorylates ubiquitin predominantly in astrocytes. npj Parkinson's Disease 5:29.

Calabresi P, Mercuri NB, Sancesario G, Bernardi G (1993) Electrophysiology of dopamine-denervated striatal neurons. Implications for Parkinson's disease. Brain 116 (Pt 2):433–452. [PubMed: 8096420]

Cheng H-C, Ulane CM, Burke RE (2010) Clinical progression in Parkinson disease and the neurobiology of axons. Annals of neurology 67:715–725. [PubMed: 20517933]

Chung W-S, Allen NJ, Eroglu C (2015) Astrocytes Control Synapse Formation, Function, and Elimination. Cold Spring Harbor Perspectives in Biology 7:a020370. [PubMed: 25663667]

Corkrum M, Covelo A, Lines J, Bellocchio L, Pisansky M, Loke K, Quintana R, Rothwell PE, Lujan R, Marsicano G, Martin ED, Thomas MJ, Kofuji P, Araque A (2020) Dopamine-Evoked Synaptic Regulation in the Nucleus Accumbens Requires Astrocyte Activity. Neuron 105:1036–1047. [PubMed: 31954621]

Creed RB, Goldberg MS (2019) Analysis of α-Synuclein Pathology in PINK1 Knockout Rat Brains. Frontiers in Neuroscience 12:1034. [PubMed: 30686993]

Creed RB, Menalled L, Casey B, Dave KD, Janssens HB, Veinbergs I, Van Der Hart M, Rassoulpour A, Goldberg MS (2019) Basal and Evoked Neurotransmitter Levels in Parkin, DJ-1, PINK1 and LRRK2 Knockout Rat Striatum. Neuroscience 409:169–179. [PubMed: 31029729]

Dagda RK, Pien I, Wang R, Zhu J, Wang KZQ, Callio J, Banerjee TD, Dagda RY, Chu CT (2014) Beyond the mitochondrion: cytosolic PINK1 remodels dendrites through Protein Kinase A. Journal of Neurochemistry 128:864–877. [PubMed: 24151868]

Dave KD et al. (2014) Phenotypic characterization of recessive gene knockout rat models of Parkinson's disease. Neurobiology of disease 70:190–203. [PubMed: 24969022]

De Haas R, Heltzel LCMW, Tax D, Van Den Broek P, Steenbreker H, Verheij MMM, Russel FGM, Orr AL, Nakamura K, Smeitink JAM (2019) To be or not to be Pink(1): contradictory findings in an animal model for Parkinson's Disease. Brain Communications.

Dehorter N, Lozovaya N, Mdzomba BJ, Michel FJ, Lopez C, Tsintsadze V, Tsintsadze T, Klinkenberg M, Gispert S, Auburger G, Hammond C (2012) Subthalamic Lesion or Levodopa Treatment Rescues Giant GABAergic Currents of PINK1-Deficient Striatum. Journal of Neuroscience 32:18047–18053. [PubMed: 23238720]

Dobrunz LE, Stevens CF (1997) Heterogeneity of release probability, facilitation, and depletion at central synapses. Neuron 18:995–1008. [PubMed: 9208866]

Du F, Yu Q, Yan S, Hu G, Lue L-F, Walker DG, Wu L, Yan SF, Tieu K, Yan SS (2017) PINK1 signalling rescues amyloid pathology and mitochondrial dysfunction in Alzheimer's disease. Brain 140:3233–3251. [PubMed: 29077793]

Emmanouilidou E, Melachroinou K, Roumeliotis T, Garbis SD, Ntzouni M, Margaritis LH, Stefanis L, Vekrellis K (2010) Cell-Produced -Synuclein Is Secreted in a Calcium-Dependent Manner by Exosomes and Impacts Neuronal Survival. Journal of Neuroscience 30:6838–6851. [PubMed: 20484626]

Feligioni M, Mango D, Piccinin S, Imbriani P, Iannuzzi F, Caruso A, De Angelis F, Blandini F, Mercuri NB, Pisani A, Nistico R (2016) Subtle alterations of excitatory transmission are linked to presynaptic changes in the hippocampus of PINK1-deficient mice. Synapse (New York, NY) 70:223–230.

Gittis AH, Hang GB, LaDow ES, Shoenfeld LR, Atallah BV, Finkbeiner S, Kreitzer AC (2011) Rapid target-specific remodeling of fast-spiking inhibitory circuits after loss of dopamine. Neuron 71:858–868. [PubMed: 21903079]

Grant LM, Kelm-Nelson CA, Hilby BL, Blue KV, Paul Rajamanickam ES, Pultorak JD, Fleming SM, Ciucci MR (2015) Evidence for early and progressive ultrasonic vocalization and oromotor deficits

in a PINK1 gene knockout rat model of Parkinson's disease. Journal of neuroscience research 93:1713–1727. [PubMed: 26234713]

Gray EG (1969) Electron microscopy of excitatory and inhibitory synapses: a brief review. Prog Brain Res. 31:141–55. [PubMed: 4899407]

Guatteo E, Rizzo FR, Federici M, Cordella A, Ledonne A, Latini L, Nobili A, Viscomi MT, Biamonte F, Landrock KK, Martini A, Aversa D, Schepisi C, D'Amelio M, Berretta N, Mercuri NB (2017) Functional alterations of the dopaminergic and glutamatergic systems in spontaneous alpha-synuclein overexpressing rats. Experimental neurology 287:21–33. [PubMed: 27771352]

Gubellini P, Picconi B, Bari M, Battista N, Calabresi P, Centonze D, Bernardi G, Finazzi-Agrò A, Maccarrone M (2002) Experimental Parkinsonism Alters Endocannabinoid Degradation: Implications for Striatal Glutamatergic Transmission. The Journal of Neuroscience 22:6900–6907. [PubMed: 12177188]

Hallett PJ, Collins TL, Standaert DG, Dunah AW (2008) Biochemical fractionation of brain tissue for studies of receptor distribution and trafficking. Current protocols in neuroscience Chapter 1:Unit 1.16.

Heeman B, Van Den Haute C, Aelvoet SA, Valsecchi F, Rodenburg RJ, Reumers V, Debyser Z, Callewaert G, Koopman WJH, Willems PHGM, Baekelandt V (2011) Depletion of PINK1 affects mitochondrial metabolism, calcium homeostasis and energy maintenance. Journal of cell science 124:1115–1125. [PubMed: 21385841]

Hunnicutt BJ, Jongbloets BC, Birdsong WT, Gertz KJ, Zhong H, Mao T (2016) A comprehensive excitatory input map of the striatum reveals novel functional organization. eLife 5.

Imbriani P, Tassone A, Meringolo M, Ponterio G, Madeo G, Pisani A, Bonsi P, Martella G (2019) Loss of Non-Apoptotic Role of Caspase-3 in the PINK1 Mouse Model of Parkinson's Disease. Int J Mol Sci 20:3407.

Kane LA, Lazarou M, Fogel AI, Li Y, Yamano K, Sarraf SA, Banerjee S, Youle RJ (2014) PINK1 phosphorylates ubiquitin to activate Parkin E3 ubiquitin ligase activity. The Journal of cell biology 205:143–153. [PubMed: 24751536]

Kitada T, Pisani A, Porter DR, Yamaguchi H, Tscherter A, Martella G, Bonsi P, Zhang C, Pothos EN, Shen J (2007) Impaired dopamine release and synaptic plasticity in the striatum of PINK1-deficient mice. Proceedings of the National Academy of Sciences of the United States of America 104:11441–11446. [PubMed: 17563363]

Kravitz AV, Freeze BS, Parker PRL, Kay K, Thwin MT, Deisseroth K, Kreitzer AC (2010) Regulation of parkinsonian motor behaviours by optogenetic control of basal ganglia circuitry. Nature 466:622–626. [PubMed: 20613723]

Lazarou M, Sliter DA, Kane LA, Sarraf SA, Wang C, Burman JL, Sideris DP, Fogel AI, Youle RJ (2015) The ubiquitin kinase PINK1 recruits autophagy receptors to induce mitophagy. Nature 524:309–314. [PubMed: 26266977]

Madeo G, Schirinzi T, Martella G, Latagliata EC, Puglisi F, Shen J, Valente EM, Federici M, Mercuri NB, Puglisi-Allegra S, Bonsi P, Pisani A (2014) PINK1 heterozygous mutations induce subtle alterations in dopamine-dependent synaptic plasticity. Movement Disorders 29:41–53. [PubMed: 24167038]

Martella G, Platania P, Vita D, Sciamanna G, Cuomo D, Tassone A, Tscherter A, Kitada T, Bonsi P, Shen J, Pisani A (2009) Enhanced sensitivity to group II mGlu receptor activation at corticostriatal synapses in mice lacking the familial parkinsonism-linked genes PINK1 or Parkin. Experimental neurology 215:388–396. [PubMed: 19071114]

Matikainen-Ankney BA, Kezunovic N, Mesias RE, Tian Y, Williams FM, Huntley GW, Benson DL (2016) Altered Development of Synapse Structure and Function in Striatum Caused by Parkinson's Disease-Linked LRRK2-G2019S Mutation. Journal of Neuroscience 36:7128–7141. [PubMed: 27383589]

McCarthy MM, Moore-Kochlacs C, Gu X, Boyden ES, Han X, Kopell N (2011) Striatal origin of the pathologic beta oscillations in Parkinson's disease. Proceedings of the National Academy of Sciences 108:11620–11625.

McCollum LA, Walker CK, Roche JK, Roberts RC (2015) Elevated Excitatory Input to the Nucleus Accumbens in Schizophrenia: A Postmortem Ultrastructural Study. Schizophrenia Bulletin 41:1123–1132. [PubMed: 25817135]

Perez-Costas E, Gandy JC, Melendez-Ferro M, Roberts RC, Bijur GN (2010) Light and Electron Microscopy Study of Glycogen Synthase Kinase-3β in the Mouse Brain. PloS one 5:e8911. [PubMed: 20111716]

Rango M, Dossi G, Squarcina L, Bonifati C (2020) Brain mitochondrial impairment in early-onset Parkinson's disease with or without PINK1 mutation. Movement Disorders. 35:504–507. [PubMed: 31898835]

Ren X, Hinchie A, Swomley A, Powell DK, Butterfield DA (2019) Profiles of brain oxidative damage, ventricular alterations, and neurochemical metabolites in the striatum of PINK1 knockout rats as functions of age and gender: Relevance to Parkinson disease. Free Radical Biology and Medicine 143:146–152. [PubMed: 31401305]

Roberts RC, Roche JK, McCullumsmith RE (2014) Localization of excitatory amino acid transporters EAAT1 and EAAT2 in human postmortem cortex: A light and electron microscopic study. Neuroscience 277:522–540. [PubMed: 25064059]

Schirinzi T, Madeo G, Martella G, Maltese M, Picconi B, Calabresi P, Pisani A (2016) Early synaptic dysfunction in Parkinson's disease: Insights from animal models. Movement Disorders 31:802–813. [PubMed: 27193205]

Scott D, Roy S (2012) -Synuclein Inhibits Intersynaptic Vesicle Mobility and Maintains Recycling-Pool Homeostasis. Journal of Neuroscience 32:10129–10135. [PubMed: 22836248]

Singh A, Mewes K, Gross RE, Delong MR, Obeso JA, Papa SM (2016) Human striatal recordings reveal abnormal discharge of projection neurons in Parkinson's disease. Proceedings of the National Academy of Sciences 113:9629–9634.

Speed HE, Dobrunz LE (2009) Developmental changes in short-term facilitation are opposite at temporoammonic synapses compared to Schaffer collateral synapses onto CA1 pyramidal cells. Hippocampus 19:187–204. [PubMed: 18777561]

Spillantini MG, Crowther RA, Jakes R, Hasegawa M, Goedert M (1998) alpha-Synuclein in filamentous inclusions of Lewy bodies from Parkinson's disease and dementia with lewy bodies. Proceedings of the National Academy of Sciences of the United States of America 95:6469–6473. [PubMed: 9600990]

Spillantini MG, Schmidt ML, Lee VM, Trojanowski JQ, Jakes R, Goedert M (1997) Alpha-synuclein in Lewy bodies. Nature 388:839–840. [PubMed: 9278044]

Stauch KL, Villeneuve LM, Purnell PR, Ottemann BM, Emanuel K, Fox HS (2016a) Loss of Pink1 modulates synaptic mitochondrial bioenergetics in the rat striatum prior to motor symptoms: concomitant complex I respiratory defects and increased complex II-mediated respiration. Proteomics Clinical applications 10:1205–1217. [PubMed: 27568932]

Stauch KL, Villeneuve LM, Purnell PR, Pandey S, Guda C, Fox HS (2016b) SWATH-MS proteome profiling data comparison of DJ-1, Parkin, and PINK1 knockout rat striatal mitochondria. Data in brief 9:589–593. [PubMed: 27761515]

Sun J, Kouranova E, Cui X, Mach RH, Xu J (2013) Regulation of dopamine presynaptic markers and receptors in the striatum of DJ-1 and Pink1 knockout rats. Neurosci Lett 557 Pt B:123–128. [PubMed: 24157858]

Sun J, Wang L, Bao H, Premi S, Das U, Chapman ER, Roy S (2019) Functional cooperation of α-synuclein and VAMP2 in synaptic vesicle recycling. Proceedings of the National Academy of Sciences 116:11113–11115.

Sun L, Shen R, Agnihotri SK, Chen Y, Huang Z, Büeler H (2018) Lack of PINK1 alters glia innate immune responses and enhances inflammation-induced, nitric oxide-mediated neuron death. Scientific reports 8:383. [PubMed: 29321620]

Surmeier DJ, Schumacker PT, Guzman JD, Ilijic E, Yang B, Zampese E (2017) Calcium and Parkinson's disease. Biochemical and Biophysical Research Communications 483:1013–1019. [PubMed: 27590583]

Tang KC, Low MJ, Grandy DK, Lovinger DM (2001) Dopamine-dependent synaptic plasticity in striatum during in vivo development. Proceedings of the National Academy of Sciences 98:1255–1260.

Tritsch Sabatini (2012) Dopaminergic Modulation of Synaptic Transmission in Cortex and Striatum. Neuron 76:33–50. [PubMed: 23040805]

Truban D, Hou X, Caulfield TR, Fiesel FC, Springer W (2017) PINK1, Parkin, and Mitochondrial Quality Control: What can we Learn about Parkinson's Disease Pathobiology? Journal of Parkinson's disease 7:13–29.

Valente EM, Salvi S, Ialongo T, Marongiu R, Elia AE, Caputo V, Romito L, Albanese A, Dallapiccola B, Bentivoglio AR (2004a) PINK1 mutations are associated with sporadic early-onset parkinsonism. Annals of neurology 56:336–341. [PubMed: 15349860]

Valente EM et al. (2004b) Hereditary early-onset Parkinson's disease caused by mutations in PINK1. Science 304:1158–1160. [PubMed: 15087508]

Villeneuve LM, Purnell PR, Boska MD, Fox HS (2016) Early Expression of Parkinson's Disease-Related Mitochondrial Abnormalities in PINK1 Knockout Rats. Molecular neurobiology 53:171–186. [PubMed: 25421206]

Volta M, Beccano-Kelly DA, Paschall SA, Cataldi S, Macisaac SE, Kuhlmann N, Kadgien CA, Tatarnikov I, Fox J, Khinda J, Mitchell E, Bergeron S, Melrose H, Farrer MJ, Milnerwood AJ (2017) Initial elevations in glutamate and dopamine neurotransmission decline with age, as does exploratory behavior, in LRRK2 G2019S knock-in mice. eLife 6.

Wang L, Das U, David Tang Y, Pamela Roy S (2014) α-Synuclein Multimers Cluster Synaptic Vesicles and Attenuate Recycling. Current Biology 24:2319–2326. [PubMed: 25264250]

Warmus BA, Sekar DR, McCutchen E, Schellenberg GD, Roberts RC, McMahon LL, Roberson ED (2014) Tau-mediated NMDA receptor impairment underlies dysfunction of a selectively vulnerable network in a mouse model of frontotemporal dementia. The Journal of neuroscience 34:16482–16495. [PubMed: 25471585]

Wilson C, Kawaguchi Y (1996) The origins of two-state spontaneous membrane potential fluctuations of neostriatal spiny neurons. The Journal of Neuroscience 16:2397–2410. [PubMed: 8601819]

Highlights:

- PINK1 knockout (KO) rats have decreased striatal dopamine tone at 4 months of age
- PINK1 KO rats have increased glutamate release onto spiny projection neurons (SPNs)
- Increased frequency and amplitude of spontaneous EPSCs onto PINK1 KO SPNs
- Increased excitatory and inhibitory synapses in PINK1 KO striatum measured by EM
- Decreased α-synuclein in glutamatergic terminals in PINK 1 KO striatum

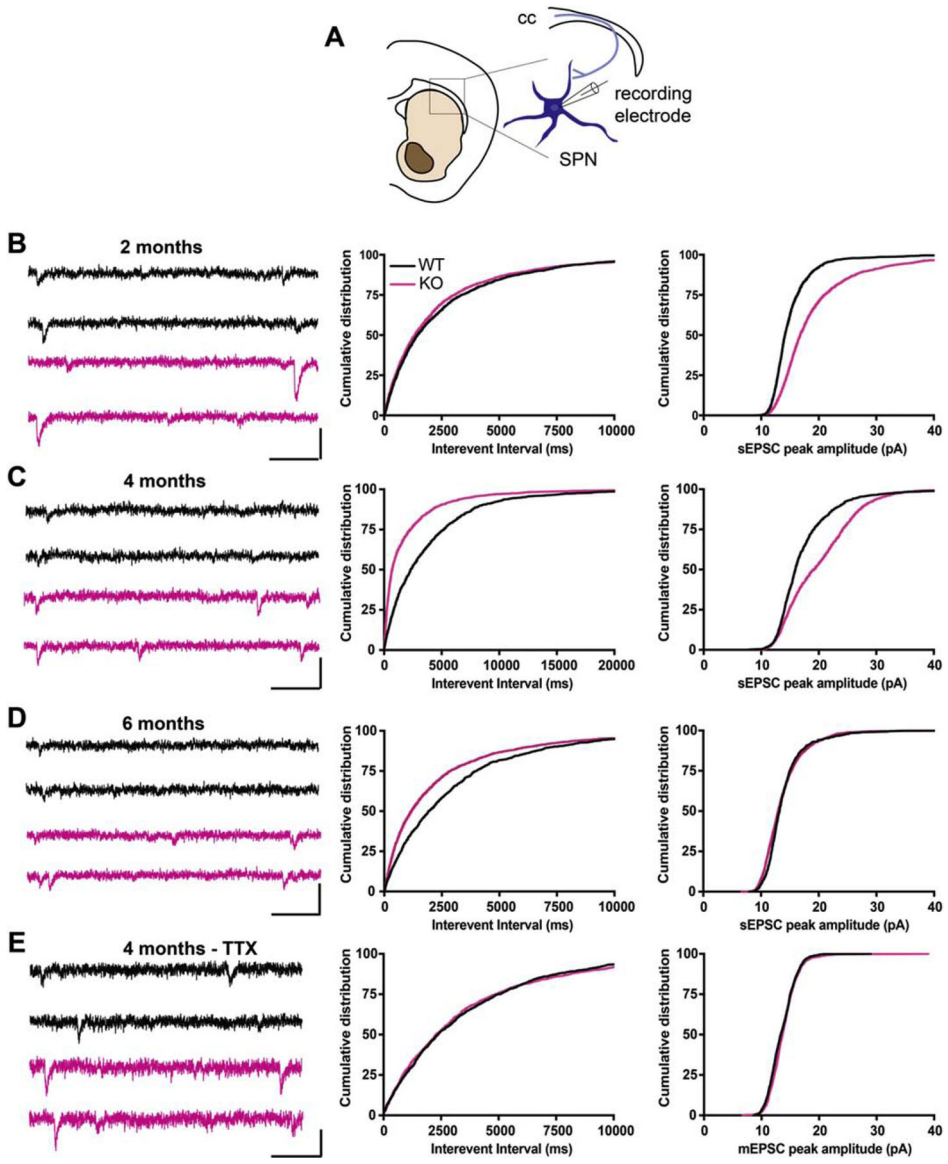

Figure 1. Increased frequency and amplitude of sEPSC in SPNs of *Pink1* KO rats.

(A) Schematic of whole-cell sEPSC recording from SPNs in the dorsal striatum. **(B)** Age 2 month WT (black) and *Pink1* KO (Pink) representative sEPSC traces (left). Cumulative probability of interevent interval (IEI) at age 2 months shows a significant increase in *Pink1* KOs compared to WTs (center; Kolmogorov- Smirnov (KS) D value 0.04239, $p<0.05$). Cumulative probability of sEPSC amplitude at 2 months shows significant increase (right; KS D value: 0.3259, $p<0.0001$) in KO compared to WT. WT: N= 7 (14 cells), KO: N=7 (17 cells). **(C)** Age 4 month WT and *Pink1* KO representative sEPSC traces (left). Decrease in the sEPSC IEI (leftward shift in the cumulative probability) indicating an increase in frequency (center) and increase in sEPSC amplitude (rightward shift in cumulative probability) (right) at 4 months in *Pink1* KO compared to WTs (KS D value: 0.2992 (IEI), 0.2575 (amplitude), $p< 0.0001$), WT: N=6 (13 cells), KO: N= 5 (12 cells). **(D)** Age 6 month WT and *Pink1* KO representative sEPSC traces (right). Decrease in the sEPSC IEI (leftward

shift in the cumulative probability curve) indicating an increase in frequency in *Pink1* KO compared to WT (center; KS D value: 0.1508, p< .0001) with a detectable change in amplitude (right; KS D value: 0.09832, p<0.0001), WT: N= 4 (9 cells), KO: N= 7 (16 cells). **(E)** Age 4 month representative mEPSC traces (left; TTX 1μM was used to block sodium channels). No change was detected in IEI between WT and *Pink1* KO rats (center; KS D value: 0.03444, p>0.05), while there was a slight but significant increase in amplitude in *Pink1* KO compared to WT (right; p<0.0001, KS D value: 0.08191), WT: N= 5 (11), KO: 7 (15 cells). Scale bars for 2, 4 and 6 month traces (B–D) = 10pA, 100ms. Sale bar for E = 5pA, 100ms.

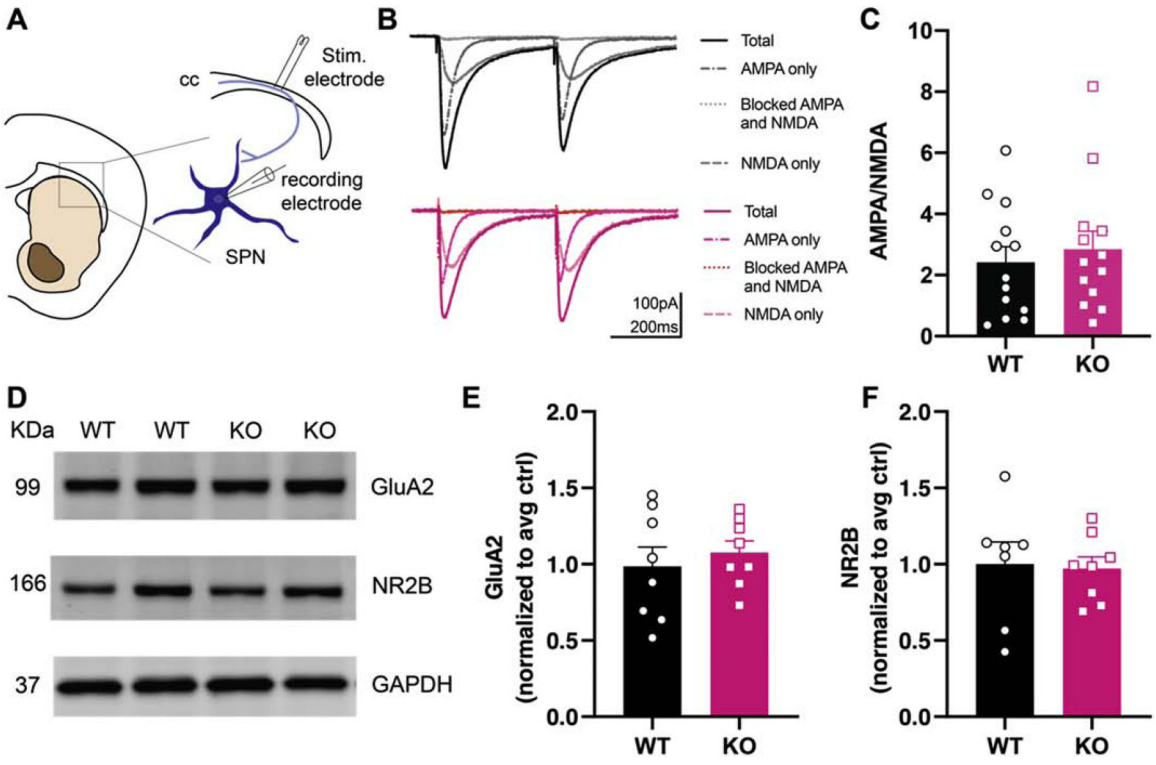

Figure 2. No change in the AMPAR/NMDAR ratio or receptor subunit expression of AMPARs and NMDARs in WT and *Pink1* KO rats at age 4 months.

(A) Recording schematic of evoked EPSC recordings from SPNs at the dorsal striatum. The stimulating electrode was placed in the corpus callosum (cc) and recordings were obtained from SPNs parallel to the stimulating electrode. **(B)** Representative traces of AMPAR and NMDAR currents from SPNs in age 4 month WT (black) and *Pink1* KO rats (Pink). **(C)** Quantification of AMPAR/NMDAR current ratio showed no change ($p > 0.05$) between WT and *Pink1* KOs, WT: N= 6 (13 cells), KO: N= 5 (13 cells). **(D)** Representative western blots of the AMPAR subunit, GluA2, the NMDA receptor subunit, NR2B, and the loading control GAPDH. **(E–F)** No changes were detected in the relative protein expression of AMPARs and NMDARs, N= 8 WT, 8 KO. $p > 0.05$, unpaired Student's t-test.

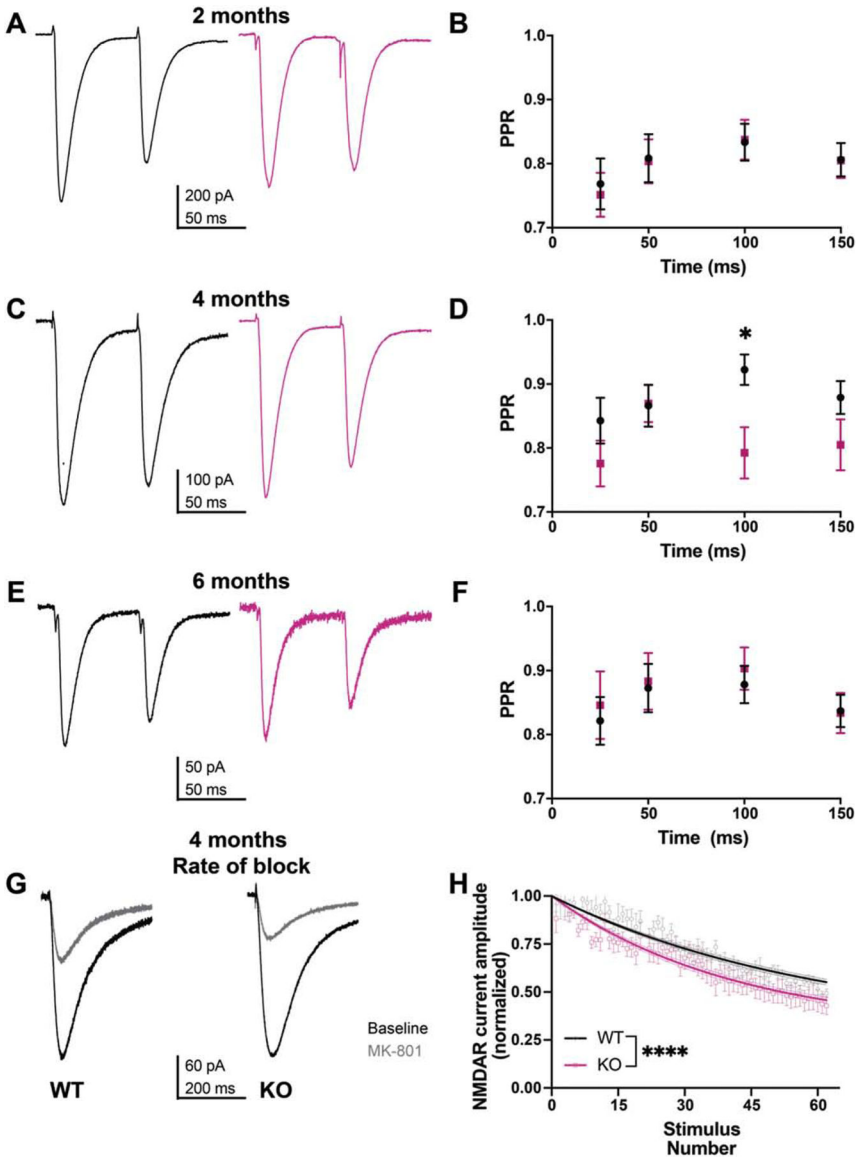

Figure 3. Increased pre-synaptic release probability in *Pink1* KO rats at age 4 months compared to WT littermate controls.

(A) Representative pairs of eEPSC traces from WT (black) and *Pink1* KO (pink) rats at 2 months. **(B)** No change in PPR in *Pink1* KO glutamatergic presynaptic terminals compared to WT littermate controls at 2 months, p> 0.05, Repeated measures two-way ANOVA. WT: 7 (14 cells), KO: 10 (18 cells). **(C)** Representative PPR traces from WT and *Pink1* KO rats at 4 months. **(D)** Increased PPR at excitatory synapses un recordings from SPNs from *Pink1* KO glutamatergic presynaptic terminals compared to WT littermate controls at age 4 months, Repeated measures two-way ANOVA, Time x Genotype interaction, $F_{(3,27)} = 3.284$, p= 0.0256; Sidak's multiple comparison p= 0.0278 at 100ms, N= 5 (13 cells) WT, N= 6 (13 cells) KOs. **(E)** Representative PPR traces from WT and PINK1 KO rats at 6 months. **(F)** No change in PPR in WT and *Pink1* KO rats, p> 0.05 Two-way AVOVA, N= 5 (11 cells) WT, N= 6 (13 cells) KO. **(G)** Representative traces of WT and *Pink1* KO rats at baseline (blacks) and following application of MK-801 (red). **(H)** NMDAR current amplitudes were

normalized to baseline, then fitted with a first order exponential (one phase decay). Curved fits were compared and showed a significant difference, $p<0.0001$, nonlinear regression analysis, Best fit values: WT: K= 0.01652, Y= 1.0, Half-life= 41.96, Span= 0.7000; KO: K= 0.02406, Y = 1.0, Half-life= 28.81, Span= 0.7000. WT: N= 5, n=9 cells; KO: N=5, n= 8 cells. K: rate constant, Y= time when X is zero, Half-time: ln(2)/K, Span: difference between Y_0 and plateau. *$p < 0.05$, ***$p<0.0001$, were considered statistically significant.

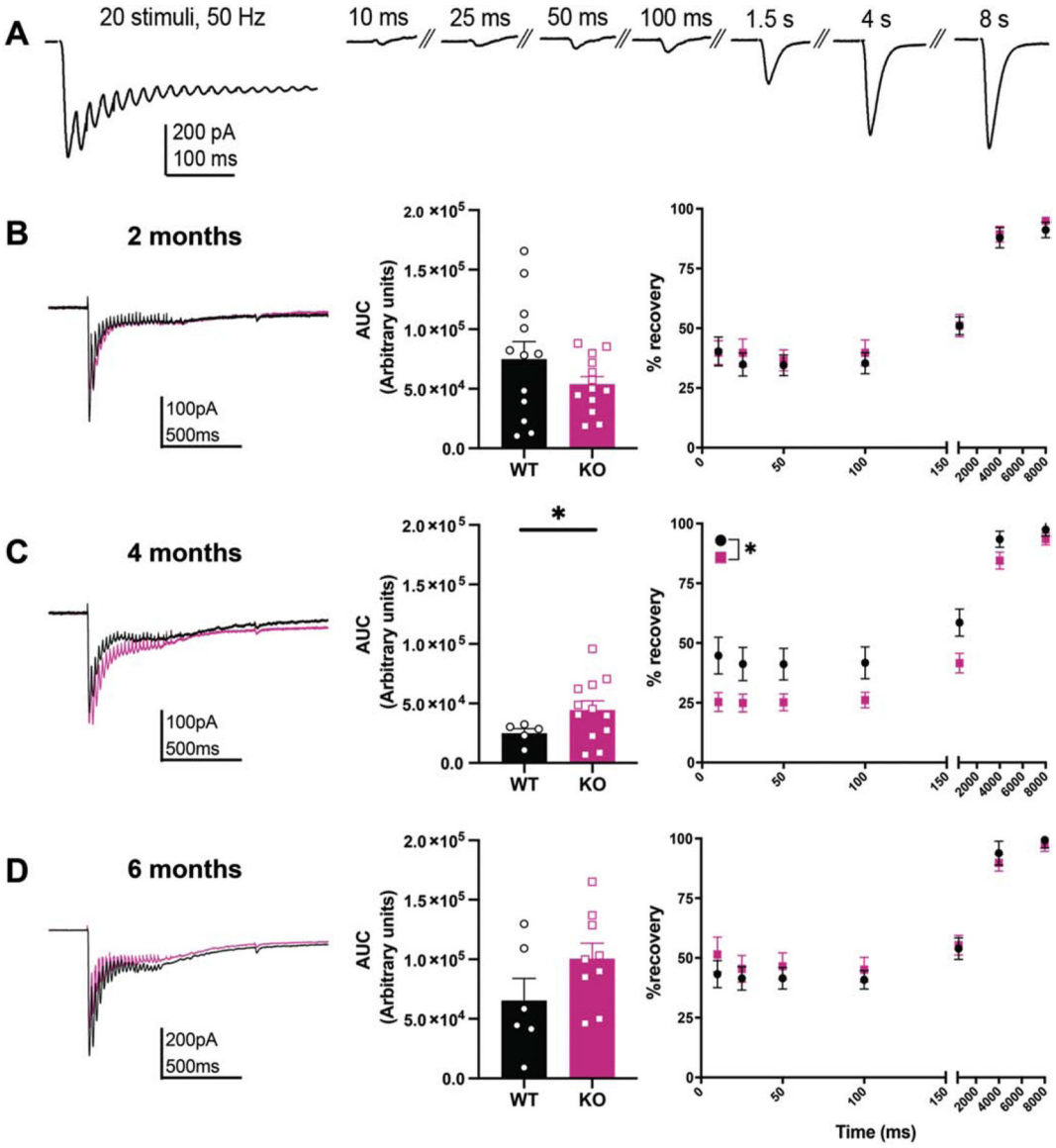

Figure 4. Increased maximum current generated by stimulus train and impaired synaptic recovery in *Pink1* KO rats at 4 months.

(A) Representative average trace illustrating the 50 Hz stimulation train and single eEPSCs at 10, 25, 50, 100ms, 1.5, 4, and 8s to measure recovery from synaptic depletion from WT and *Pink1* KO rat SPN at 2, 4, and 6 months. **(B)** Representative trace during 50Hz train at 2 months (left). Bar graph shows no change in maximum current generated (area under the curve, AUC) by the stimulus train between WT and PINK1 KO rats (center: WT: N= 6 (12 cells), KO N=6 (13 cells)). Scatter plot shows no change in % recovery following synaptic depletion by train stimulation between WT and *Pink1* KO rats (right; WT N=6 (14 cells), KO: N=6 (14 cells)). **(C)** Representative trace during 50 Hz train at 4 months (left). Maximum current generated by the stimulus train is significantly increased in *Pink1* KO rats compared to WT rats (p= 0.0368; unpaired Student's t-test with Welch's correction; WT: N= 4, n= 4 cells, KO: N= 4, n=12 cells), followed by a lesser % recovery of evoked amplitude in *Pink1* KO rats (Repeated measures two-way ANOVA, Time x Genotype interaction:

$F_{(6, 132)}$= 2.775, p= 0.0142; main effect of genotype: $F_{(1,22)}$= 5.445, p= 0.0292) compared to WT controls, WT: N= 4 (13), KO: N= 4 (11 cells). **(D)** Representative trace during 50Hz train at 6 months (left). No changes were detected in maximum current generated by the stimulus train (center; WT: N= 4 (6 cells), KO: 4 (9 cells)) or % recovery (right; WT: N= 4 (8 cells), KO N=4 (12 cells)) in *Pink1* KO compared to WT rats. *p< 0.05, were considered statistically significant.

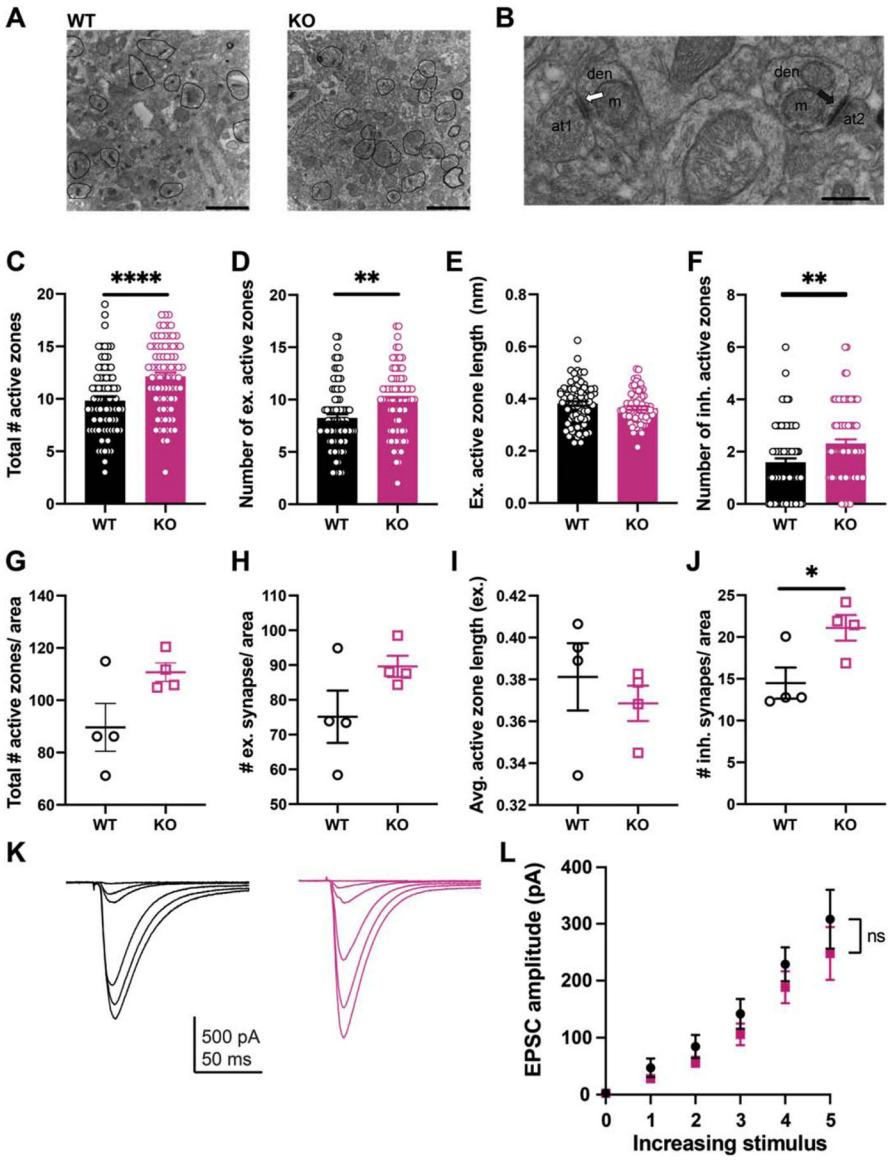

Figure 5. Increased number of active zones with similar synaptic strength in the striatum of 4 month old *Pink1* KO rats.

(A) Electron micrographs of synapses in WT and *Pink1* KO rats. Each individual synapse is circled. Scale bars=2 μm. **(B)** Higher power image showing examples of different types of synapses. An axon terminal (at1) forms an inhibitory synapse (white arrow) onto the dendrite (den). Another terminal (at2) forms an excitatory synapse (black arrow) onto the dendrite. Note that the post synaptic densities of excitatory synapses (black arrow) are much thicker than that of the inhibitory synapse (white arrow). Scale bar =500nm. **(C)** Total number of active zones is greater in *Pink1* KO rats compared to WT littermate controls, $p<0.0001$, Student's t-test. **(D)** There was a greater number of excitatory synaptic active zones in PINK1 KO rats compared to WT, $p= 0.009$, Mann Whitney U test. **(E)** There were no detectable changes in excitatory active zone length in WT compared to *Pink1* KO rats. **(F)** There was a greater number of inhibitory synaptic active zones active zones in *Pink1* KO rats compared to WT littermate controls, $p= 0.0012$, Mann Whitney U. **(G)** Total number of

active zones per area was averaged per animal and showed no difference between WT and *Pink1* KO rats. **(H)** Number of excitatory active zones per area was averaged per animal and showed no difference between WT and *Pink1* KO rats. **(I)** Length of excitatory (ex.) active zone per area averaged per animal showed no difference between WT and *Pink1* KO rats. **(J)** Number of inhibitory active zones per area was averaged per animal and showed a greater number in *Pink1* KO rats compared to WT littermate controls, p=0.0336, unpaired Student's t-test. For distributions, n= 80 micrographs for each group (WT and KO), for averages, N= 4 rats each per group (WT and KO). p> 0.05. **(K)** representative traces from an input-output curve for WT (black) and *Pink1* KO rats (pink). **(L)** No changes in eESPC amplitude with increasing stimulus strength between WT and KO, p> 0.05, Repeated measures two-way ANOVA, WT: N= 6 (13 cells), KO: N= 4 (11 cells). *p<0.05, **p<0.01, ***p<0.001, ****p<0.0001, were considered significant.

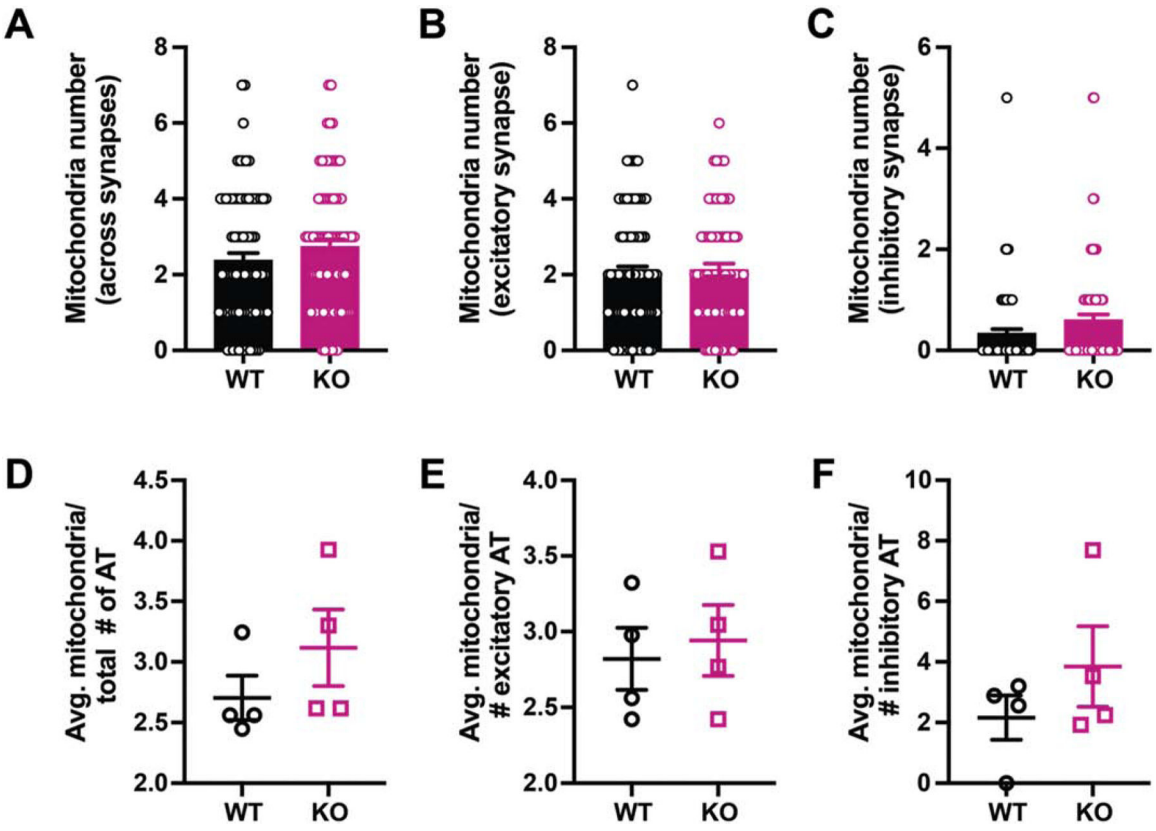

Figure 6. Similar number of presynaptic mitochondria in WT and *Pink1* KO rats at 4 months.

(A) Total number of mitochondria across all synapses showed no difference between *Pink1* KO rats compared to WT littermate controls. **(B)** Similar number of mitochondria at excitatory synapses in *Pink1* KO rats compared to WT littermate controls. **(C)** Similar number of mitochondria at inhibitory synapses in *Pink1* KO rats compared to WT littermate controls. **(D)** Average number of mitochondria per the total number of axon terminals showed no difference between WT and *Pink1* KOs. Average number of mitochondria per number of excitatory axon terminals **(E)** and inhibitory axon terminals **(F)** showed no difference between WT and P *Pink1* KOs. For A–C, n= 80 micrographs for each group (WT and KO), for D–F, N= 4 rats each per group (WT and KO). p> 0.05.

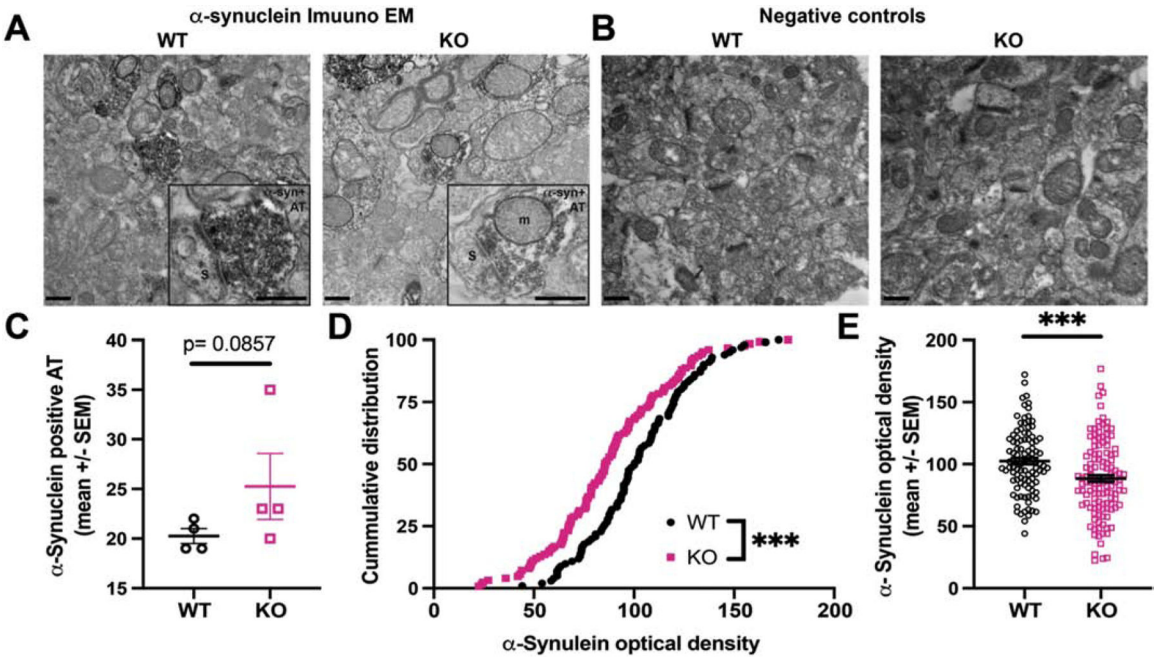

Figure 7. Presynaptic α- synuclein immunoreactivity in the dorsal striatum of 4 month old WT and *Pink1* KO rats.

(A) WT and *Pink1* KO striatal tissue immunostained for α- synuclein. s- indicates spines, m- mitochondria, AT- axon terminals. Boxed insets show zoomed in areas of α-synuclein positive presynaptic terminals **(B)** Negative control (no primary antibody) striatal tissue shows no α-synuclein immunoreactivity in WT or KO rats. **(C)** No difference in the average number of α- synuclein positive axon terminals in WT and *Pink1* KO rats, N= 4 WT, 4 KOs **(D)** Cumulative distribution of α- synuclein optical density shows a decrease (leftward shift) in *Pink1* KO rats compared to WT controls ($p < 0.001$, Kolmogorov-Smirnov test, D value = 0.2752). (E) Average α-synuclein optical density was decreased in *Pink1* KO rats compared to WT controls ($p < 0.001$, Unpaired Student's t-test). Optical density was measured from 101 WT and 125 KO α-synuclein positive axon terminals. *p<0.05, ***p< 0.01 were considered statistically significant. Scale bars=500 nm.

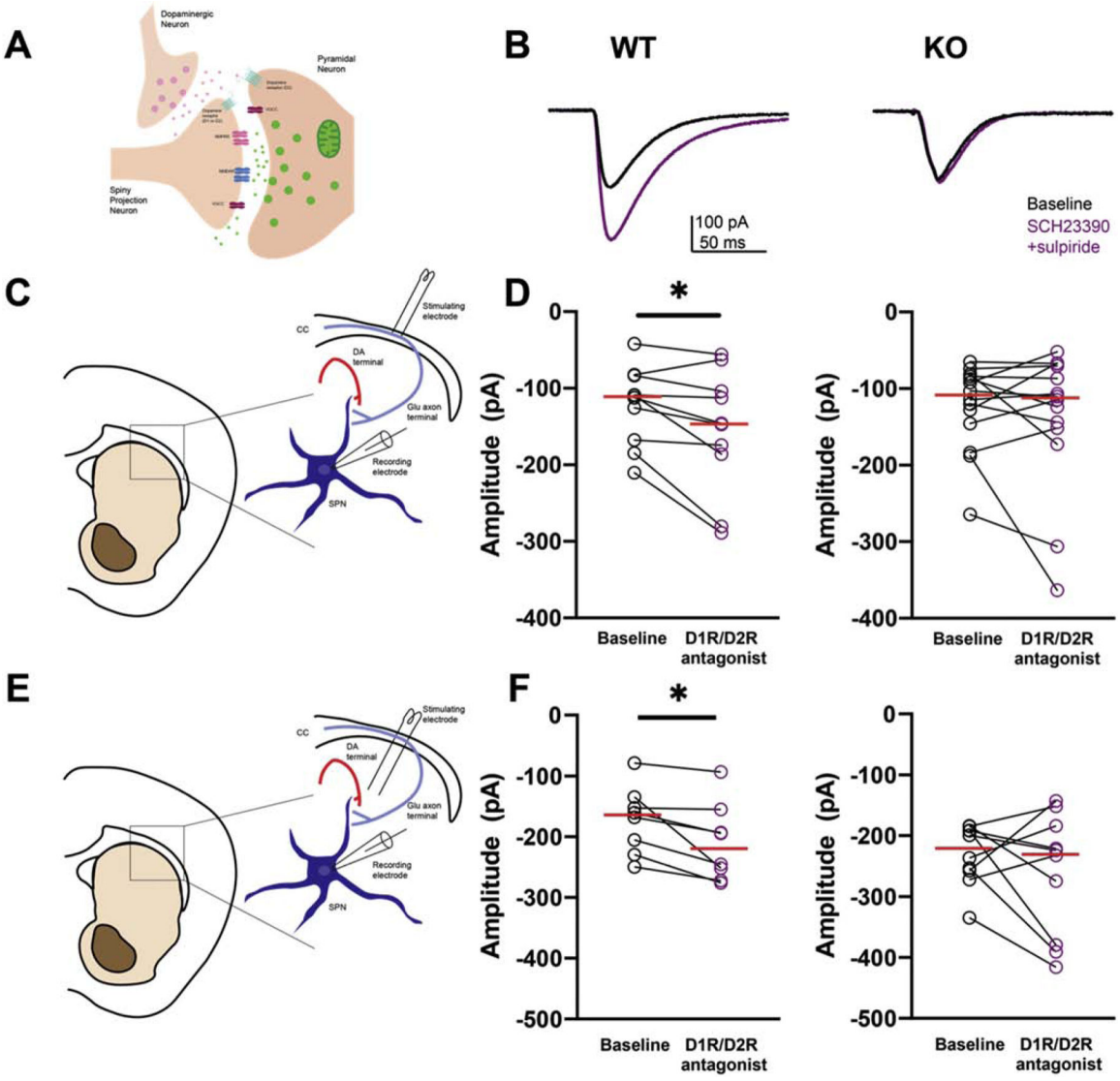

Figure 8. Inhibition of striatal dopamine receptors reveals altered response to dopamine receptor antagonism in *Pink1* KO rats compared to WT littermate controls at 4 months.

(A) Schematic of dopamine signaling in the dorsal striatum. **(B)** Representative eEPSCs at baseline (black) vs after 15 minute application of SCH23390 (3μM) and sulpiride (10μM) (purple) to block D1 and D2 receptors respectively, from WT and *Pink1* KO rats. **(C)** Recording schematic of eEPSC recordings from SPNs at the dorsal striatum. Stimulating electrode was placed in the corpus callosum and recordings were obtained from SPNs parallel to the stimulating electrode. **(D)** WT SPNs showed a net increase in eEPSC amplitude following D1R/D2R inhibition (p= 0.0220, paired t-test, N= 6 (10 cells) WT pairs) while no net change in eEPSC amplitude was detected in SPNs from *Pink1* KO rats (p> 0.05, paired t-test, N =7 (14 cells) KO pairs). **(E)**. Recording schematic of eEPSC recordings from SPNs at the dorsal striatum. Stimulating electrode was placed in dorsal striatum and recordings were obtained from SPNs parallel to the stimulating electrode. **(F)** WT SPNs showed a net increase in eEPSC amplitude following inhibition with dopamine receptor antagonist cocktail (p = 0.0186, paired t-test, N= 3(8 cells) WT pairs) compared to

no detectable net change in eEPSC amplitude from *Pink1* KO ($p > 0.05$, paired t-test, N= 3 (10 cells) KO pairs). *$p < 0.05$ was considered statistically significant.